Regional detection and monitoring of injection-induced seismicity: Application to the 2010–2012 Youngstown, Ohio, seismic sequence

S. G. Holtkamp, M. R. Brudzinski, and B. S. Currie

ABSTRACT

Increased rates of seismicity in tectonically quiescent regions like the midcontinent region of the United States have been hypothesized to be related to human activities such as oil and gas production and wastewater injection. It can be difficult to establish how human activities relate to earthquakes, particularly when local seismic networks are not available to provide a high-quality characterization of the seismic sequence in question. Here, we use a multistation waveform crosscorrelation approach to evaluate the relationships between earthquakes associated with the 2011–2012 Youngstown, Ohio, seismic sequence and the injection history of a local wastewater disposal well. By using data recorded by four regional seismic stations 50–200 km (31–124 mi) away from Youngstown, we demonstrate that high-resolution results can be achieved without using costly and scientifically focused local seismic deployments. Compared to the number of events recorded using standard detection methodologies, we realize a 25-fold increase in detected seismicity (282 detected events) during the sequence, and allow us with confidence to interpret a direct link between seismicity and well injection volumes. Using a combination of absolute and relative location techniques, we demonstrate that seismicity migrated from below the injection well toward the west, along a line consistent with a nodal plane of the largest earthquake in the sequence. We are able to separate the seismic sequence into three distinct phases, consistent with changes in injection rates and maximum injection pressures. In addition, using daily injection volume records, we can identify two families of similar earthquakes. The first family occurred

Manuscript received December 12, 2013; provisional acceptance October 3, 2014; revised manuscript received February 25, 2015; final acceptance March 31, 2015.
DOI: 10.1306/03311513194

AUTHORS

S. G. Holtkamp ~ *Department of Geology and Environmental Earth Science, Miami University, Oxford, Ohio; present address: Geophysical Institute, University of Alaska Fairbanks, Fairbanks, Alaska; sgholtkamp@alaska.edu*

Stephen Holtkamp earned an M.S. degree from Cornell University and a Ph.D. from Miami University. He was a post-doc at the University of Alaska Fairbanks (UAF) before joining UAF as a research seismologist in 2015. His research focuses on earthquake swarms, including induced seismicity. He received the AAPG George C. Matson Memorial Award in 2014 for the material presented in this manuscript.

M. R. Brudzinski ~ *Department of Geology and Environmental Earth Science, Miami University, Oxford, Ohio; brudzimr@miamioh.edu*

Michael Brudzinski earned a Ph.D. from the University of Illinois and received an endowed postdoctoral fellowship at the University of Wisconsin before joining Miami University in 2004. His research focuses on earthquake origins, ranging from subduction zone tremor in Mexico to induced seismicity in the United States. He and Brian Currie formed GeoSeismic Analytics, LLC, to provide additional private consulting to industry.

B. S. Currie ~ *Department of Geology and Environmental Earth Science, Miami University, Oxford, Ohio; curriebs@miamioh.edu*

Brian Currie received a B.S. degree from Allegheny College, an M.S. degree from the University of Rochester, and a Ph.D. from the University of Arizona. He was a post-doc at the University of Chicago before joining Miami University in 2000. His research areas include depositional systems, sequence stratigraphy, stable-isotope paleoaltimetry, petroleum geology, and the tectonics of sedimentary basins.

ACKNOWLEDGEMENTS

This research was supported by Michael Brudzinski's NSF CAREER grant no. 0847688. Geophysical log interpretation software used in this study was supplied by the LMKR University Grant Program. We would like to thank members of the Ohio Department of Natural Resources Division of Geological Survey and the OhioSeis Ohio Seismic Network (particularly Michael Hansen and James McDonald) for conducting a thorough initial investigation and inviting us to participate in an informative discussion. Stations M54A and N54A, which we found to be essential to the quality of our results, are Earthscope Transportable Array stations that were installed early with permanent status to become part of the Advanced National Seismic System (ANSS) backbone network. Stations ACSO and MCWV are operated by the United States Geological Survey as part of the ANSS backbone array. We also benefited from the publication of a report by the Lamont-Doherty Earth Observatory, and from discussions with Danielle Sumy, Honn Kao, and Justin Rubenstein.

DATASHARE 65

Table S1 is available in an electronic version on the AAPG Web site (www.aapg.org/datashare) as Datashare 65.

early in the sequence and close to the injection well and was followed by a recurrence pattern that lagged injection activity by 1 day. The second family. which occurred later in the sequence and farther from the well, displayed a 4-day lag. We interpret these relationships to be related to pore-pressure diffusion rates within the fault network responsible for the seismicity. Collectively, our technique shows the high quality of results possible when only a few regional seismic stations are available for monitoring.

INTRODUCTION

Induced seismicity, here defined as earthquakes directly caused by human activity, has been documented and studied through both controlled experiments (Raleigh et al., 1976; Zoback and Harjes, 1997) and related to industry activities (Hitzman et al., 2012). Earthquakes have been attributed to a variety of human activities including oil and gas production, wastewater injection, mining, reservoir filling, and geothermal energy development (McGarr et al., 2002; Ake et al., 2005; Deichmann and Giardini, 2009; Hitzman et al., 2012) and have occurred throughout a broad range of geologic settings (Nicholson and Wesson, 1992). Not only do induced earthquakes have direct hazard potential (Keranen et al., 2013), but they also have an impact on the public's perception of the environmental impacts of activities linked to seismic events. Earthquakes induced by petroleum-industry-related activities seem to be rare, with only a handful of confirmed cases despite the hundreds of thousands of wells associated with hydrocarbon production and wastewater disposal in the United States (Hitzman et al., 2012). Because of the relatively low magnitude of induced seismic events and the lack of dense networks of local seismic monitoring stations, it is likely that most induced earthquakes are unrecorded (Seeber et al., 2004). Because of this lack of resolution, the pervasiveness of induced seismicity in the United States is unknown. The observation that many "felt" induced seismic events have lower magnitude precursors (Shapiro et al., 2011; Kim, 2013) justifies the need for a more thorough examination of the continuously recorded seismic data available from regional seismic networks in the United States (Frohlich, 2012).

Recent studies have observed an increase in small magnitude seismicity in the midcontinent region of the United States (Horton, 2012; Ellsworth, 2013; Keranen et al., 2013). It has been hypothesized that this seismicity is related to recent increases in the volume of wastewater, primarily derived from hydraulic fracturing during oil and gas well completions, that has been injected into deep saline aquifers in the region (Ellsworth, 2013).

The leading hypothesis to explain this relationship is that injected wastewater may increase pore fluid pressures in existing faults and fractures in rocks within or adjacent to subsurface injection intervals. As pore fluid pressure increases, the effective normal stress acting on a fault surface is reduced, and if optimally oriented with respect to the regional tectonic stress field, slip along the fault surface may produce a recorded seismic event (Simpson, 1986; Nicholson and Wesson, 1990; Zoback and Harjes, 1997). The likelihood of this scenario is further enhanced if a fault exists in a state that is already close to failure (Townend and Zoback, 2000). Alternately, injection may be affecting local shear stress in an elastic sense to bring a fault closer to failure, but generally the mass of injected liquids is too low to have a profound effect on seismicity (Simpson, 1986). Because a smaller volume of fluid is required to affect stresses in the pore-pressure hypothesis, seismicity patterns could change abruptly as the pore-pressure front interacts with the fault zone (Shapiro et al., 2002).

Studies of injection-induced seismicity have provided many observations that strongly support the reduced normal stress hypothesis (Zoback and Harjes, 1997; Shapiro et al., 2003). However, these studies benefited from extensive prior planning and involved deploying closely spaced local seismometer networks or deep borehole seismometers around specific wells or within fields with well-monitored injection histories (Zoback and Harjes, 1997; Dorbath et al., 2009). Although these studies have been successful in relating fluid pressure diffusion to earthquake activity, it is not reasonable to install or expect similar observational capabilities at each of the hundreds of thousands of well sites throughout the United States. Below, we propose a new methodology for approaching investigations of induced seismicity that does not rely upon local seismic data, using earthquakes of the 2010–2012 Youngstown, Ohio, seismic sequence as a test case.

THE 2010–2012 YOUNGSTOWN, OHIO, SEISMIC SEQUENCE

On March 17, 2011, the Ohio Department of Natural Resources Ohio Seismic Network (ODNR OSN) (Hansen and Ruff, 2003) recorded a pair of small earthquakes of magnitude 2.1 and 2.6 (M2.1 and M2.6) in Youngstown, Ohio. Although active seismicity in the Youngstown area had not been previously recorded, small earthquakes such as these are not uncommon to intraplate regions like the Midwest (Zoback, 1992). However, between August and December 2011, the OSN recorded nine additional earthquakes of similar magnitude. This uncommon persistence of events led to speculation that the earthquakes were being caused by activity at the D&L Energy 1 Northstar Class II wastewater disposal well (API 3409923127), which began operating in late December 2010. To more fully delineate the nature of the recorded events, the ODNR, in collaboration with the Lamont-Doherty Earth Observatory of Columbia University, deployed a small local seismic network in December 2011. Preliminary data obtained from this deployment indicated that the earthquakes were occurring within Proterozoic crystalline basement rocks below the injection well (ODNR, 2012), suggesting that the events were induced (Kim, 2013). As a result, injection operations were suspended on December 30 (ODNR, 2012).

In this study, we investigate how the Youngstown seismic sequence in eastern Ohio is related to injection at the D&L Energy 1 Northstar well as previously suggested (ODNR, 2012; Kim, 2013; Skoumal et al., 2014). Our study differs from Kim (2013) in that we focus on regional data over the entire duration of the sequence, whereas Kim (2013) relies on the local seismic data late in the sequence.

HISTORY OF THE D&L ENERGY 1 NORTHSTAR WASTEWATER DISPOSAL WELL

Figure 1 shows the locations of the D&L Energy 1 Northstar disposal well, the earthquake epicenters associated with the Youngstown seismic sequence, related regional geologic features, historical seismicity, and the seismic network distribution used in this study. Based on well completion records on file with the ODNR, drilling of the D&L Energy 1 Northstar well occurred between April 27 and May 13, 2010. A diagram illustrating the general well characteristics

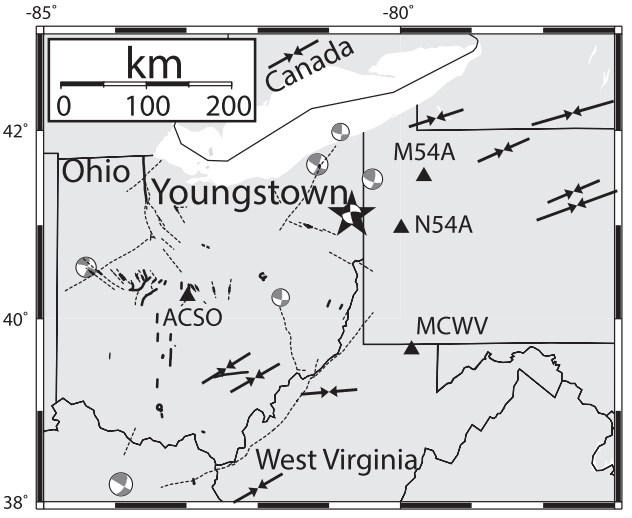

Figure 1. Basement structures (solid = known faults; dashed = faults or structural trends inferred from structural or magnetic discontinuities; from Baranoski, 2013), primary maximum compressive stress solutions (arrows, in which length scales with stress magnitude) (Mazzotti and Townend, 2010), local earthquake focal mechanisms (beach ball diagrams in bottom hemisphere projection, where shading indicates compressional quadrants, white indicates extensional quadrants, and nodal planes indicate possible fault orientations. Maximum compressive stress, the *p*-axis of the strain tensor, bisects the tensional quadrant), and broadband seismometers (triangles) used in this study. Lightly shaded focal mechanisms are historical regional seismicity (4< Mw <5) and align with the regional stress field. The black focal mechanism represents the solution for the December 31, 2011 Youngstown earthquake (ODNR, 2012).

is shown in Figure 2. The well was drilled as a 28-cm (11-in.) diameter hole to a depth of 315 m (1033 ft), where casing (22-cm [9-in.] diameter) was set and cemented into the surface. From 315 m (1033 ft) to total depth at 2802 m (9192 ft), the well was drilled with a borehole diameter of 20 cm (8 in.). The base of 14-cm (6-in.) diameter steel production casing was set at 2504 m (8215 ft) and cemented in up-hole to a depth of approximately 2161 m (7092 ft). Injection tubing (6-cm [2-in.] diameter) run from the surface was set with a packer within the production casing at 2480 m (8137 ft) (ODNR, 2012).

To facilitate wastewater injection, the lower 298 m (977 ft) of the well was completed open hole. Well completion records indicate a 238-m (780-ft) injection interval within Cambrian carbonate and siliciclastic rocks, as well as approximately 60 m (200 ft) in the underlying Precambrian crystalline basement (Figure 2). Potential injection reservoirs in the lower Paleozoic strata identified from geophysical logs include dolostones and sandstones in the Cambrian Knox Dolomite, and basal sandstone of the underlying Cambrian Conasagua Group (Figure 2).

In eastern Ohio, the Knox dolomite is subdivided into informal subsurface units including the copper ridge dolomite in the lower half of the unit (Wickstrom et al., 2005; Ryder et al., 2012). Production casing in the D&L Energy 1 Northstar well was set near the top of the copper ridge dolomite "B-zone" (Calvert, 1974), an interval of dolomitic fine-grained sandstone and siltstone (ODNR, 2012). Porosity logs indicate that approximately 10 m (32 ft) of the B-zone has porosities greater than 8% (average porosity of 9.4%). Tracer surveys of the injection interval indicate the B-zone likely served as an upper injection reservoir for the well (ODNR, 2012).

The basal sandstone of the Conasagua Group is an informal subsurface stratigraphic unit that has been historically referred to as the Mt. Simon Sandstone. Recent subsurface stratigraphic investigations, however, indicate the Mt. Simon Sandstone is primarily a western Ohio subsurface unit that pinches out in west-central Ohio (Wickstrom et al., 2005; ODNR, 2012). The basal sandstone of Conasauga Group in the D&L Energy 1 Northstar well is approximately 40-m (130-ft) thick and consists of quartz arenite with thin interbeds of dolostone and shale (ODNR, 2012). The interval contains approximately 15 m (48 ft) of greater than 8% porosity (average porosity of 10.3%). Continuous, high-porosity zones within the interval range from approximately 0.3 to 7 m (1 to 23 ft) in thickness and are generally associated with enhanced permeability as determined by a magnetic resonance log of the interval (ODNR, 2012).

Precambrian basement rocks in the well are composed of biotite-, quartz-, and feldspar-rich igneous or metamorphic rocks (ODNR, 2012). Geophysical logs indicate several zones of high porosity/permeability within the basement interval. An approximately 6-m (20-ft) zone of high-porosity/permeability straddling the Cambrian-Precambrian contact is interpreted as a Cambrian weathering horizon beneath the

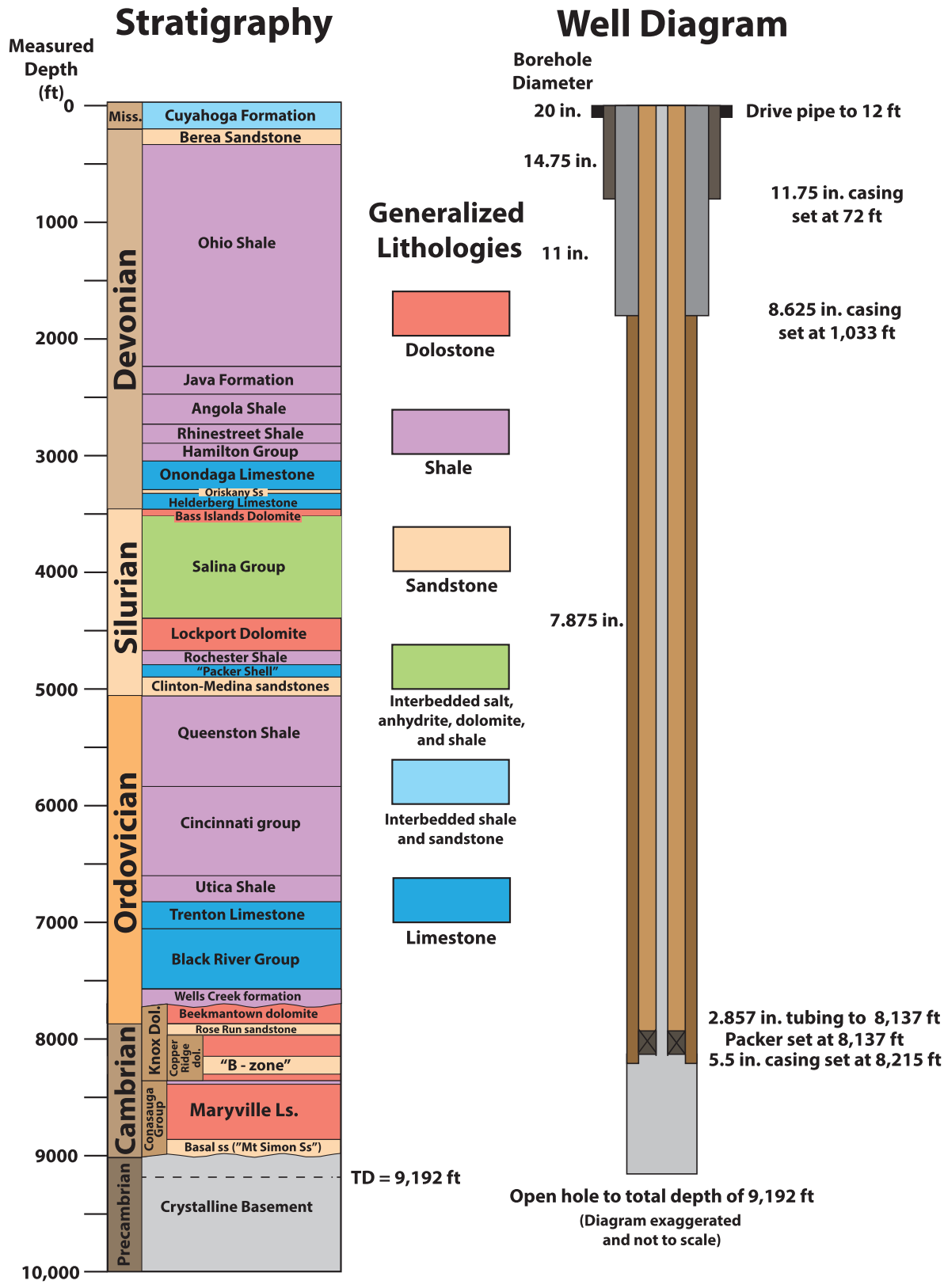

Figure 2. Stratigraphy and well construction diagram for the D&L Energy 1 Northstar Class II wastewater disposal well. Stratigraphic section includes both formal and informal stratigraphic names commonly used for the subsurface of eastern Ohio (Wickstrom et al., 2005; Baranoski, 2007; Ryder et al., 2012). Diagram modified from ODNR (2012). TD = total depth.

unconformity surface, or diagenetic alteration caused by ancient fluid migration along the basement cover contact. Additional high-permeability and high-porosity zones in the basement interval are evident on formation of geophysical logs between 2764–2769 m (9070–9086 ft) and 2773–2776 m (9097–9106 ft). In the lowermost zone, microresistivity image logs indicate the presence of high-angle fractures intersecting the borehole (ODNR, 2012).

Prior to the initiation of wastewater injection, the entire open-hole interval was treated with approximately 5680 L (1500 gal) of 28% HCl. Testing of the injection interval was conducted on June 4, 2010, and the state of Ohio approved the injection well for commercial operation on July 12, 2010. The issued permit stated that the injection interval was for the Knox-Precambrian interval and allowed a maximum injection pressure of approximately 13 MPa (1890 psi) (ODNR, 2012, Appendix 8). Commercial injection was initiated on December 28, 2010, and unlike most other potential cases of induced seismicity, daily injection volumes are available for investigation. Approval to increase maximum injection pressures to approximately 15.5 MPa (2250 psi) was granted by the state on March 16, 2011, and again to approximately 17 MPa (2500 psi) on May 3, 2011. We note that sustained daily injection volumes in excess of 2000 bbl were achieved after August 3, 2011. Throughout testing and operation of the D&L Energy 1 Northstar well, more than 496,000 bbl of wastewater were injected (ODNR, 2012).

DETAILED CHARACTERIZATION OF THE 2010–2012 YOUNGSTOWN SEISMIC SEQUENCE

Initial characterization of the Youngstown seismic sequence by the OSN was limited by traditional seismic techniques, which require an earthquake to be large enough to have multiple seismic waves visible above background noise at multiple stations. Only earthquakes larger than M2 were able to meet these requirements in the Youngstown case. To establish whether a direct causal relationship between the operating history of the injection well and the entire Youngstown seismic sequence exists, we developed a multiple station template matching (waveform crosscorrelation) algorithm (Gibbons and Ringdal, 2006; Shelly et al., 2007), which is able to detect events much smaller than those of traditional techniques. Matched filter techniques have been increasingly used recently because of this ability to detect smaller signals, and they comprise a variety of techniques including single station (Van der Elst et al., 2013) and multistation (Peng and Zhao, 2009) techniques, and stacked waveform (Shelly and Hardebeck, 2010; Van der Elst et al., 2013) techniques. Our technique uses four broadband seismometers located within 200 km (124 mi) of the earthquakes, eliminating the need for costly (and scientifically focused) local seismic deployments.

METHODOLOGY

Network matched filtering (NMF), sometimes referred to as template matching, uses the seismic recording of a known earthquake (referred to as the "template event") to identify similar earthquakes at other times through a process called crosscorrelation. The seismic recording of an earthquake is the result of a combination of three parameters: (1) the earthquake's source parameters, such as the focal mechanism and source time function; (2) the path between the earthquake and receiver, including both the network geometry and local structure of the earth including all geologic formations along the travel path from the earthquake hypocenter to the recording instruments; and (3) the receiver response function of the specific recording instrument. Because every layer in the heterogeneous earth produces its own set of reflections and refractions of passing seismic waves, even slight changes in either the source or path parameters of an earthquake (e.g., different focal mechanism or earthquake location) can result in dramatically different recorded waveforms across the network. Because the seismic stations we chose have remained unchanged for the duration of our study, we do not attempt to remove the instrument response from the seismograms.

The first step in this NMF process is identifying an earthquake (the template event) that is large

enough, approximately greater than M1.5 from our visual inspection, for the larger S-waves to be recorded on several nearby seismometers (the network), as shown in Figure 3. We then band-pass filter the template event seismograms from 1 to 12 Hz, a process that filters out low- and high-frequency noise not related to the earthquakes, to accentuate the S-wave arrivals from the template event relative to background noise. We chose a 20–s-long template length because this length encompasses the P- and S-waves at the two nearby stations, as well as the S-wave train at the farther stations. We then compute a normalized crosscorrelation (a measure of how similar two signals are to each other) of the template recording of each component at each station in the network against their respective continuous data streams. This produces a crosscorrelation stream for each channel for each template over the time processed. We found that any band-pass limits from 1 to 2 Hz on the low end and 4 to 12 Hz on the high end worked almost equally well. The normalized crosscorrelation we use seeks to match the relative amplitudes and frequencies in the template waveform and ignores absolute amplitudes. Choosing too narrow of a band-pass filter effectively removes frequency information such that matches are only because of the relative amplitude variations similar to the template. In the end, we chose a passband of 1–12 Hz, approximately 3.5 octaves, to avoid any potential problems with narrow passbands. We then sum up each crosscorrelation stream, preserving the offset between the relative template onset times at each station. This final summation greatly enhances the ability of the NMF technique to find coherent signals within the background noise (Figure 4) because the signal from multiple seismic stations stacks coherently but the noise does not. Following Shelly et al. (2007), we use the median absolute deviation (MAD) to set the detection threshold as it is a robust outlier detector. For each day, we calculate the

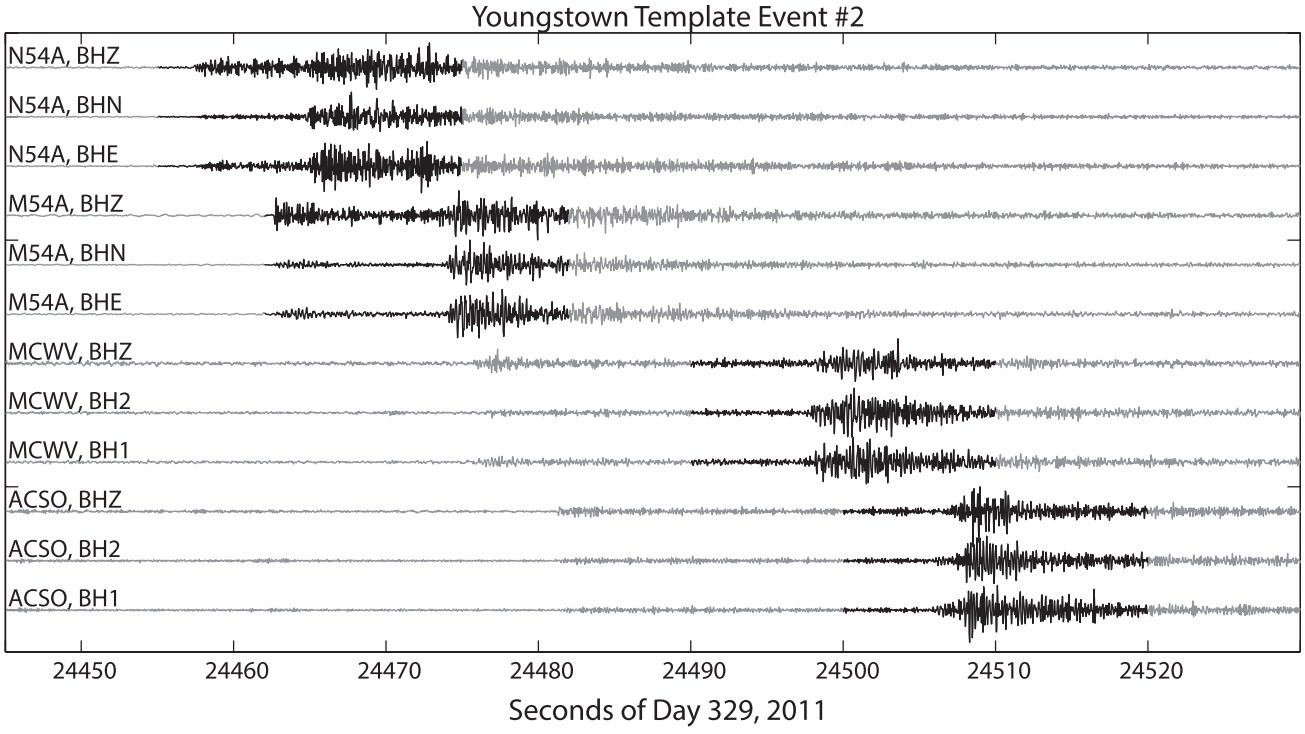

Figure 3. Example of a template Youngstown earthquake on November 25, 2011. The continuous time series is band-pass filtered from 1 to 12 Hz (gray), and we highlight the part of the waveform extracted to be the template (black). Our final results use a constant template duration of 20 s, but we find that as long as the median absolute deviation is used as the detection criteria, the duration of the templates (or uniformity of template length) does not have a significant impact on detection capabilities. The time offset between stations, as shown by the time lag between the beginning of the red sections, is preserved throughout the correlation and summation process.

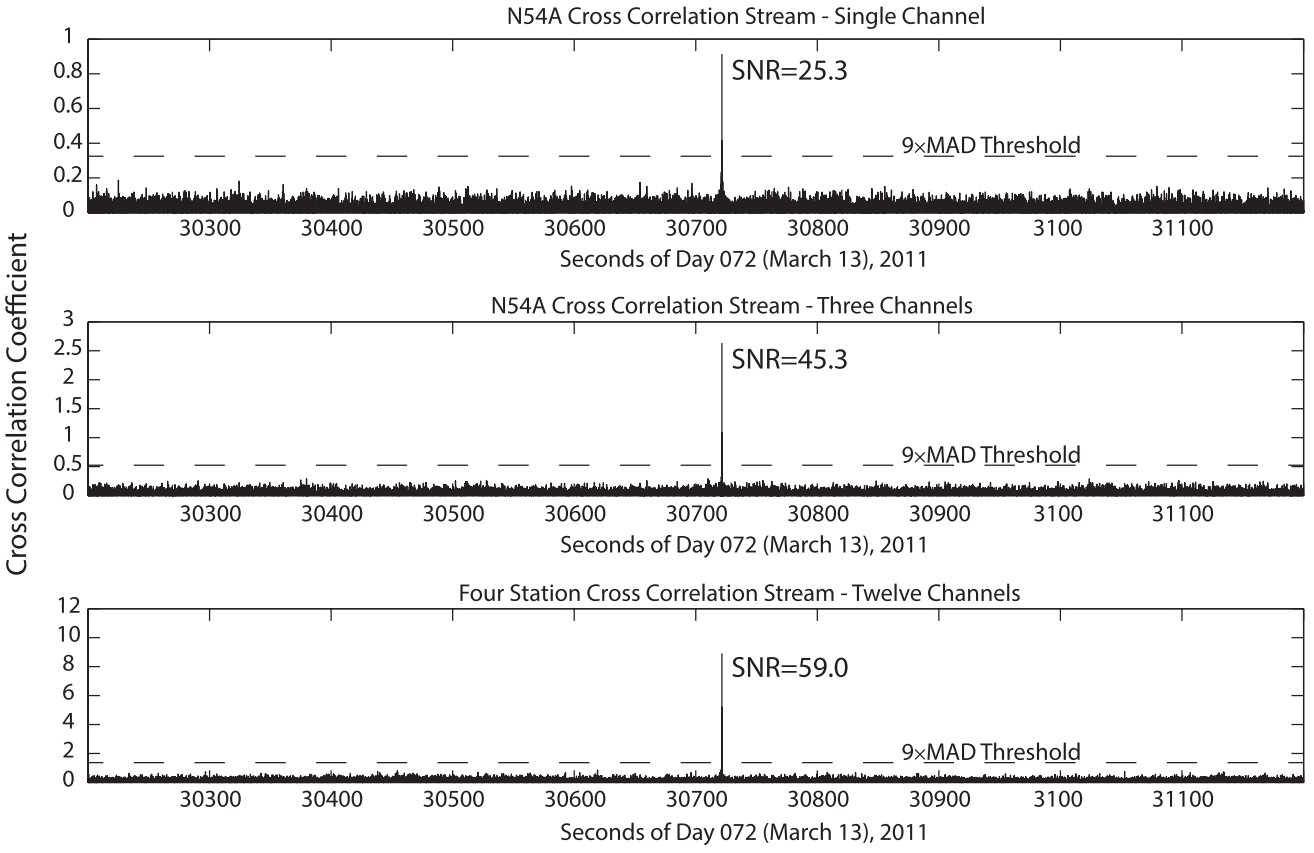

Figure 4. Demonstration of how the signal-to-noise ratio (SNR) increases with additional channels included in template matching crosscorrelation (1, 3, and 12 channels). This shows the positive detection of a M1.3 earthquake on March 13, 2011 at about 40 standard deviations above the mean when four stations are used. We define the signal to be the value of the large peak, and the noise to be the median absolute deviation (MAD) for the day. Although the SNR increases as more stations are added, there are diminishing returns, such that at some point, it is no longer advantageous to include more stations in the detector.

MAD of the crosscorrelation stream, and then we set a detection threshold at nine times this value (9 × MAD) over the mean. We chose 9 × MAD, similar to six standard deviations, because it corresponds to a false positive rate of less than one per yr (per template). Because we find hundreds of detections in approximately 2 yr of data, we are confident that our characterization of the seismic sequence is not significantly influenced by spurious detections.

In reality, a sequence of earthquakes occurs over a range of locations. Because undetected earthquakes may be occurring at some distance away from the template event, it is important to use a variety of template events (representing a range of known earthquake locations) to ensure that as many earthquakes are detected as possible. To produce this set of template events, we start by identifying a new earthquake that is not well correlated (<25 × MAD) with any prior template. We then make this new earthquake a template event and iterate this procedure until all newly detected events are well correlated with a template event. We found that only four templates (March 17, 2011 at 10:53 UTC; November 25, 2011 at 06:47 UTC; July 16, 2011 at 21:28 UTC; and September 30, 2011 at 00:52 UTC) were required to conclusively identify (at >25 × MAD) all M > 1.7 events (the threshold at which an event could be made into a template). Because of the high degree of waveform similarity among the different families of detected events, using additional events as templates past this point gives rapidly diminishing returns (Figure 5). Other less well correlated events are too small to produce a template that would yield any new events. We chose four stations to use in our

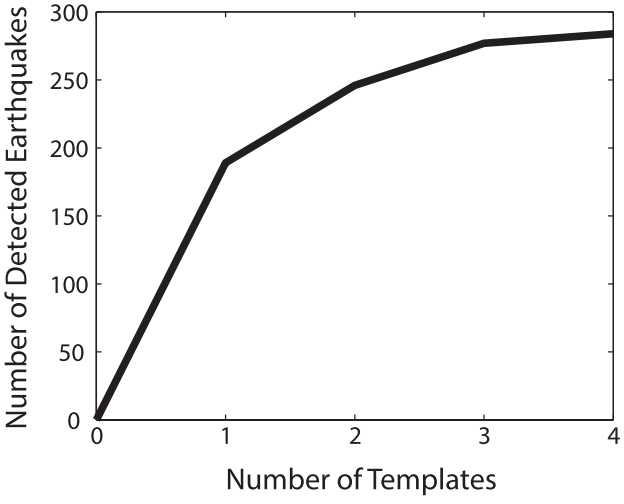

Figure 5. Illustration of diminishing returns. The additional number of detected earthquakes diminishes with each template processed, meaning it is not necessarily constructive to use each detected event as a template because of processing time constraints. This demonstrates how only a small number of templates (we use four) can produce well characterized seismic sequences.

detector (seismic stations N54A, M54A, ACSO, and MCWV) because all stations recorded continuously throughout the Youngstown sequence without equipment changes. Although our technique could produce comparable results elsewhere with similarly spaced permanent seismic stations, the nominal 70-km (43-mi) spacing afforded by the EarthScope Transportable Array seismic experiment (M54A and N54A are early Transportable Array installations) greatly increases the return of our technique and has the potential to be an integral part of investigating triggered seismicity in the United States.

This technique has the advantage that the cross-correlation value is almost completely decoupled from seismic background noise (Figure 6). Here, three earthquakes occurred on a day that had a variety of seismic noise levels, including very high-amplitude (likely cultural) noise at the end of the day. Despite the variations in seismic noise, the cross-correlation noise level remains constant throughout the day and the signal from the earthquakes is positively correlated just as effectively. This insensitivity to background noise makes our technique ideal for producing a complete time history.

To compare our earthquake catalog to the injection history, we separated the catalog by template match and converted these earthquake catalogs to daily time series. With the earthquake catalog and injection history at the same sampling interval, we then crosscorrelated those two functions to determine any correlation between them. Figure 7 shows the results of this correlation, and both families show small positive time lags, one day for template 1 and four days for template 2 (templates 3 and 4 are more ambiguous), indicating the amount of time it takes for the fluid pressure pulse to reach the earthquake source regions, presumably via pore fluid pressure diffusion. This is also apparent with a simple visual inspection of the left panels on Figure 7 in which the calculated correlation lags have been accounted for, as gaps in injection are correlated with gaps in seismicity.

RESULTS

With this technique, we detect 282 seismic events occurring between November 2010 and November 2012 (Figure 8, Table S1, supplementary material available as AAPG Datashare 65 at www.aapg.org/datashare), with an apparent magnitude of completeness (Mc, the magnitude above which all events should be reported in the catalog) of 1.0 ± 0.13 and a b-value (the constant b in the Gutenberg-Richter law, which is defined by the size distribution of earthquakes in a catalog) of 1.32 ± 0.21 (Figure 9). Because our detection criterion is based on the signals ability to sum coherently across multiple stations, each positive detection exceeds a certain degree of confidence. This confidence is what the detection threshold refers to, and is not strictly a magnitude threshold. However, even if we exclude positive detections below our completeness threshold (bringing our catalog down to 157 events), our results do not change significantly. This 25-fold increase in the characterization of the seismic sequence allows us to more directly test how seismicity is related to injected water volumes.

Our improved resolution of the seismic sequence reveals three phases, where the initial phase begins two weeks after the initiation of commercial injection operations (December 28, 2010), the second phase begins soon after injection pressures are approved to

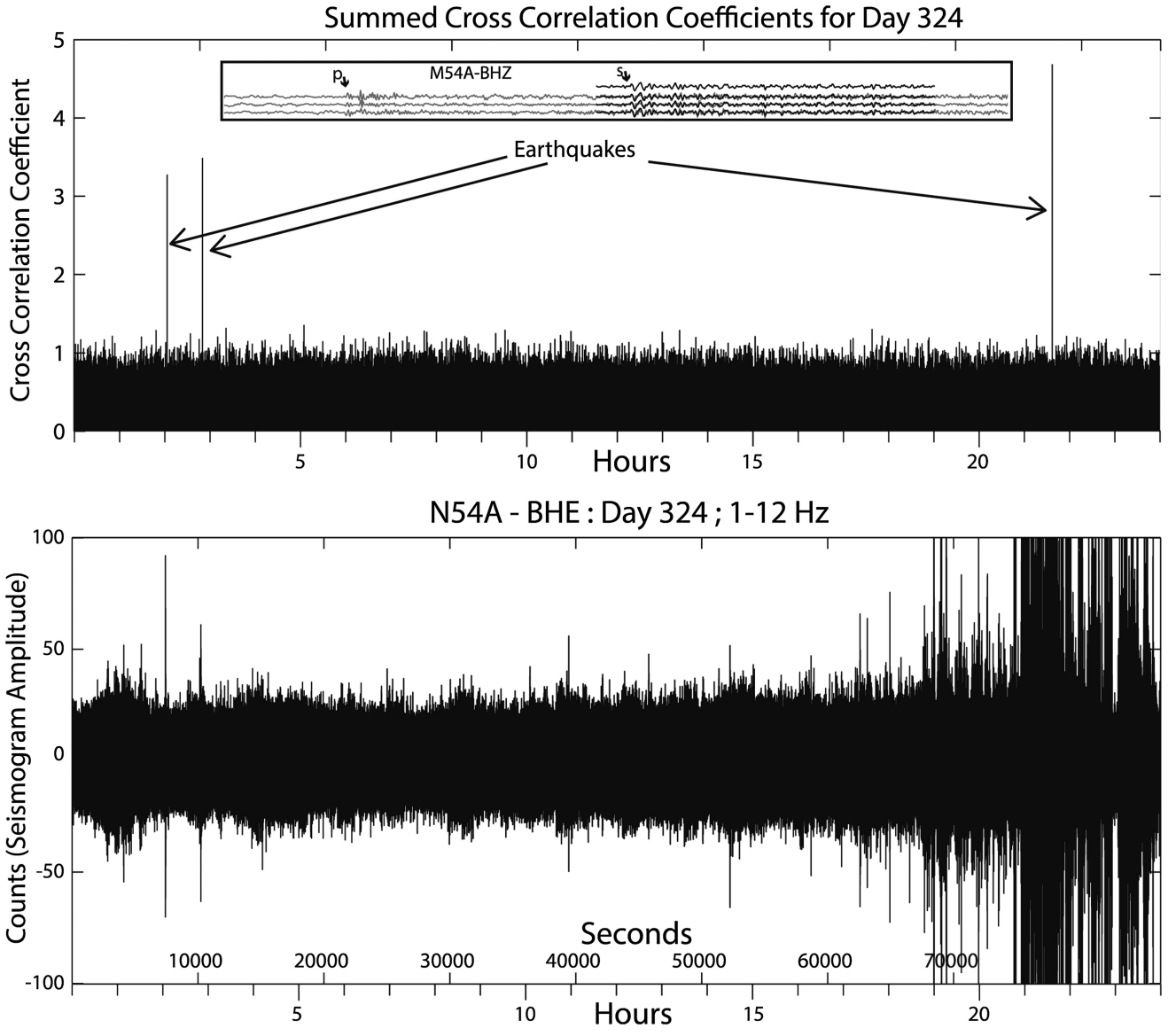

Figure 6. Example of the decorrelation between template-matching crosscorrelation (top) and the seismic noise (bottom) for November 20, 2011. The bottom panel shows a day-long band-pass filtered seismogram and demonstrates a variety of seismic noise types. In the first half of the day, the two highest amplitude signals are local earthquakes, but they are not necessarily dominant over the background noise level (bottom), which has hour-long amplitude variations. The last third of the day is dominated by noise, defined as any signal other than an earthquake similar to the template event, most likely cultural noise. Despite this large difference in background noise levels, the typical crosscorrelation coefficient remains nearly constant throughout the day (top). The three earthquakes detected on this day (arrows) are shown in the inset panel (gray = continuous seismic data; black = template waveform. The P- and S-wave arrivals are shown for these three events). This example illustrates why the crosscorrelation technique is the well-suited one to produce a complete time series of similar events. There are fewer gaps in the record because of the seismic noise.

exceed 17 MPa (2500 psi) (May 3, 2011), and the third phase begins soon after sustained daily injection volumes in excess of 2000 bbl (August 3, 2011), ending two weeks after injection ended. We refer to all earthquakes after shut-in as phase four, but note that earthquakes originating at some distance from the injection point will not respond to this shut-in until the pore-pressure "back-front" (analogous to the pore-pressure triggering front) arrives some distinct time later (Shapiro and Dinske, 2009). Our improved catalog shows that the rate of earthquakes very closely follows the injection history, with a gradual

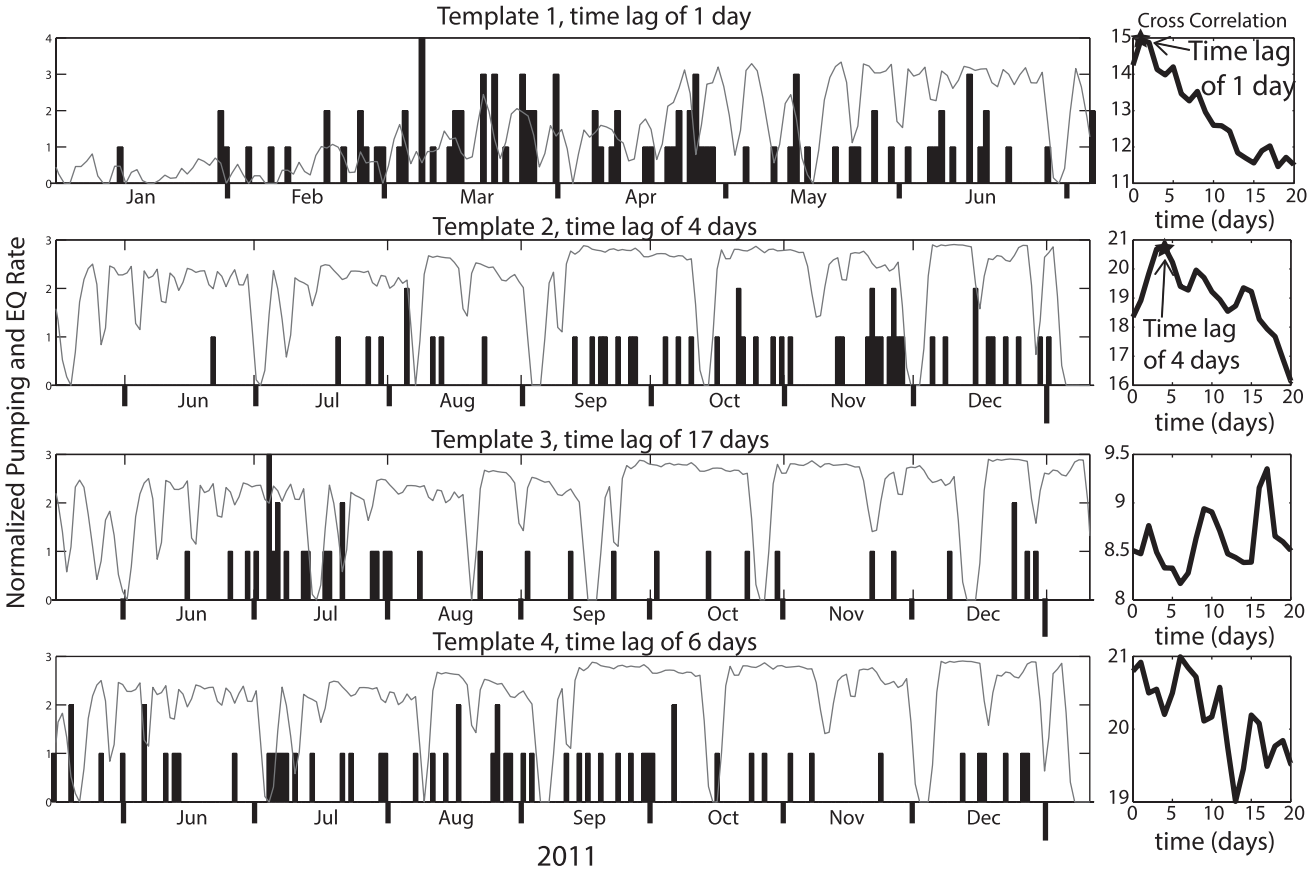

Figure 7. Evidence for a time lag between wastewater injection and earthquake triggering for the two families of events. For each family, we crosscorrelate the daily injection time series (solid line, normalized for plotting purposes) and the daily number of earthquakes (histogram, earthquakes per day) shown in the left panels, with the resulting correlation coefficients (unitless) in the right panels. If wastewater injection is causing the earthquakes, we would expect the earthquake time series to be better correlated with the injection time series at some small positive lag time. For templates 1 and 2, the peak crosscorrelation is at a small positive time lag (black star, 1 day and 4 days, respectively), indicating the amount of time it takes for the fluid pressure pulse to reach the earthquake source regions. Template 3 is ambiguous because most events occurred over a short time span, and template 4 has two similar peaks at 1 and 6 days, although the 6th day peak is stronger.

rate increase at the beginning of the sequence and an abrupt reduction in earthquake rate after injection ceased.

We find over 100 earthquakes in phase 1, although only 2 were greater than M2.0 (Figure 8A). Phase 1 consists almost entirely of earthquakes that most closely match template 1. The rate of earthquakes changes during phase 1, with a gradual rate increase during the first two months, up until about when injection pressures are approved to exceed 15.6 MPa (2250 psi) (March 15, 2011, two days before the largest events in phase 1). During phases 2 and 3, however, the cumulative seismicity shows a nearly constant linear trend that parallels the cumulative injection volume (Figure 8). We find it particularly intriguing that the constant cumulative seismicity increase is maintained between phases 2 and 3 despite a shift from more template 1 earthquakes to more template 2–4 earthquakes, perhaps indicating a change in fault behavior of template 1 as it relates to the fluid pressure pulse migrating through these earthquakes' source region and fluids start reaching the source region for later families. Earthquakes during phase 3 contain more than 99% of the overall moment release. Using the Geophysical Institute Seismology Matlab Objects (GISMO) toolbox (Reyes and West, 2011), we processed all matched waveforms through a clustering algorithm (Buurman

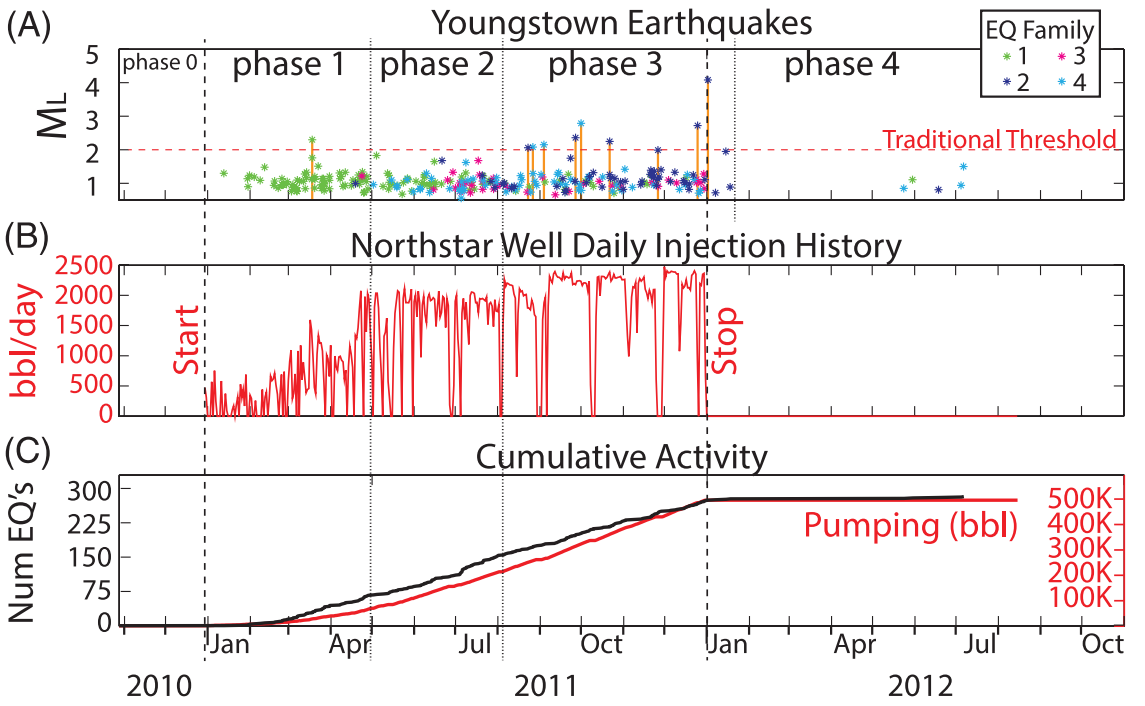

Figure 8. Time history of Youngstown earthquakes compared with injection volumes at the D&L Energy 1 Northstar well. Vertical dashed lines through all panels shows three seismicity phases defined by waveform similarity in Figure 10 that correspond to changes in injection. (A) Earthquake magnitude over time, color coded by earthquake family according to which template they most closely match. Orange solid lines indicate ODNR detected event magnitudes, and dashed red line is approximate lower detection limit of the traditional detection threshold (i.e., events below this line were not detected by standard seismic processing techniques). (B) Daily injection volumes at the D&L Energy 1 Northstar well. (C) Cumulative seismicity (black) versus cumulative injected volumes (ODNR, 2012). ML = local magnitude; EQ = earthquakes.

and West, 2010), which identifies three to five main "families" of events (Figure 10) that are consistent with the three main seismic sequence phases we observe. From this clustering analysis, we again see evidence of a multiple phase sequence, as shown in an interevent correlation matrix (Figure 11).

High-resolution studies relying on extensive local seismic networks have clearly documented triggered seismicity by pore-pressure diffusion in reservoirs by establishing an apparent relationship between distance from injection source and the timing of earthquakes initiate (Shapiro et al., 2002). This time lag, however, has only been demonstrated using a dense local array of seismometers. We attempt to identify potential time lag effects in our catalog by crosscorrelating the daily injection history with the daily earthquake occurrence for each family of earthquakes. If any correlation exists, there should be a notable peak in the crosscorrelation coefficient at some distinct positive time lag (Figure 7). Template 1, which is

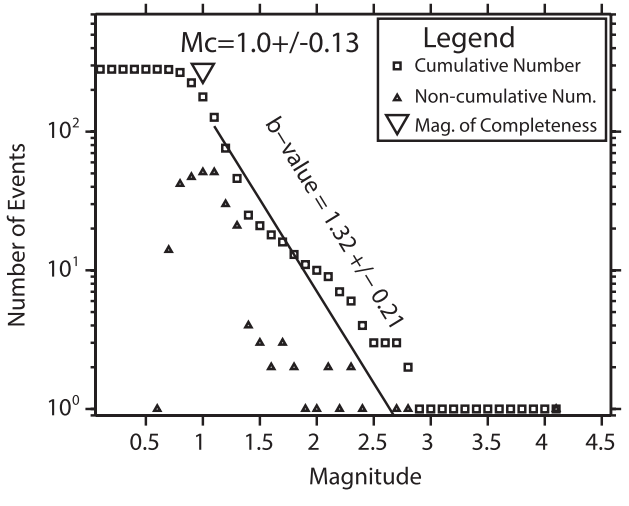

Figure 9. Results of frequency-magnitude analysis of our enhanced earthquake catalog showing a magnitude of completeness of 1.0 ± 0.13 and a *b*-value of 1.3. Symbols plotted are the cumulative number of earthquakes above a certain magnitude (squares), the total number of earthquakes at a certain magnitude (triangles), and the magnitude of completeness calculated for the catalog (upside down triangle).

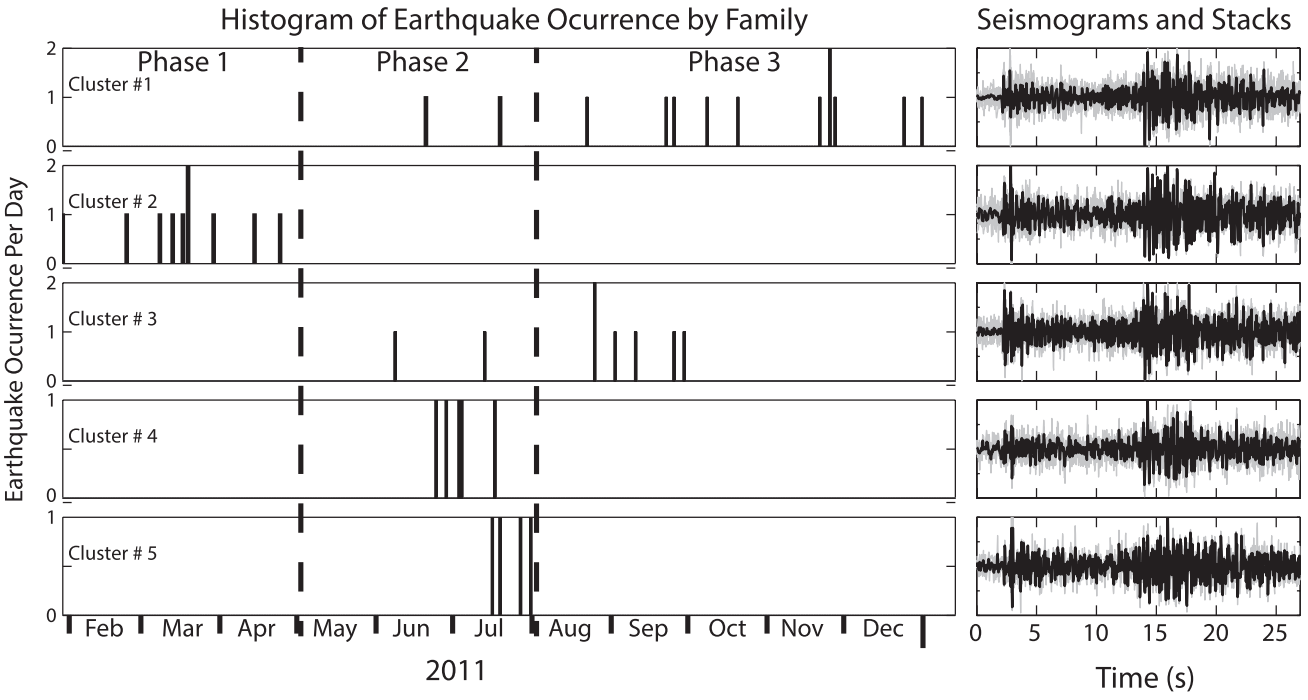

Figure 10. Clustering results from Geophysical Institute Seismology Matlab Objects (GISMO) for station-component N54A-BHE, showing that the events can be separated into two main clusters: one that dominates the early earthquakes and one that dominates the later earthquakes, as well as several smaller clusters prominent during the middle of the sequence. These clusters are defined by waveform similarity on one component of one station, a limitation of GISMO. Cluster 1 is associated with phase 1 earthquakes and cluster 2 with phase 3 earthquakes. Clusters 3, 4, and 5 start in July 2011 and likely represent phase 2 earthquakes, which may be transitional in nature. Vertical dashed lines through all panels show our approximate differentiation of the three phases of seismicity.

most prominent during phase 1, shows a clear time lag between injection and fault slip of 1 day. Templates 2 and 4, which are most prominent during phase 3, show a longer time lag of 4 and 6 days, suggesting it takes longer for injected fluid to influence a fault patch that began slipping later in the sequence of events. For a saturated homogenous medium, this corresponds to a hydraulic diffusivity, $D = 0.23\ m^2/s$, consistent with other measurements of diffusion-triggered seismicity in shallow fault zones (Shapiro et al., 2003; Parotidis, 2005; El Hariri et al., 2010). Although the M4.0 earthquake occurred the day after shut-in, the pore-pressure back-front would not have reached the source location of this earthquake yet (Parotidis, 2004).

To calculate relative earthquake locations, we again use GISMO to compute a subsample relative phase arrival lag matrix, using 0.5–1.2 s windows (depending on the station) to identify when P- and S-wave trains for each trace are arriving relative to

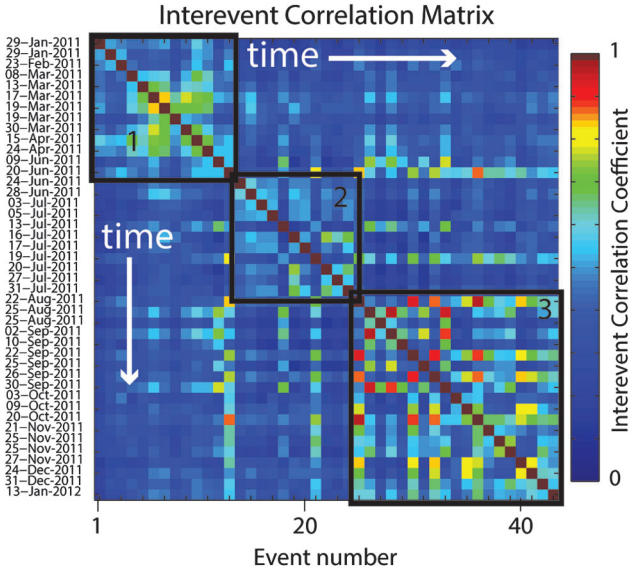

Figure 11. Interevent correlation matrix for the events is also shown in Figure 12. Warm colors represent higher degrees of waveform similarity, and blocks of warm colors indicate specific phases of the sequence.

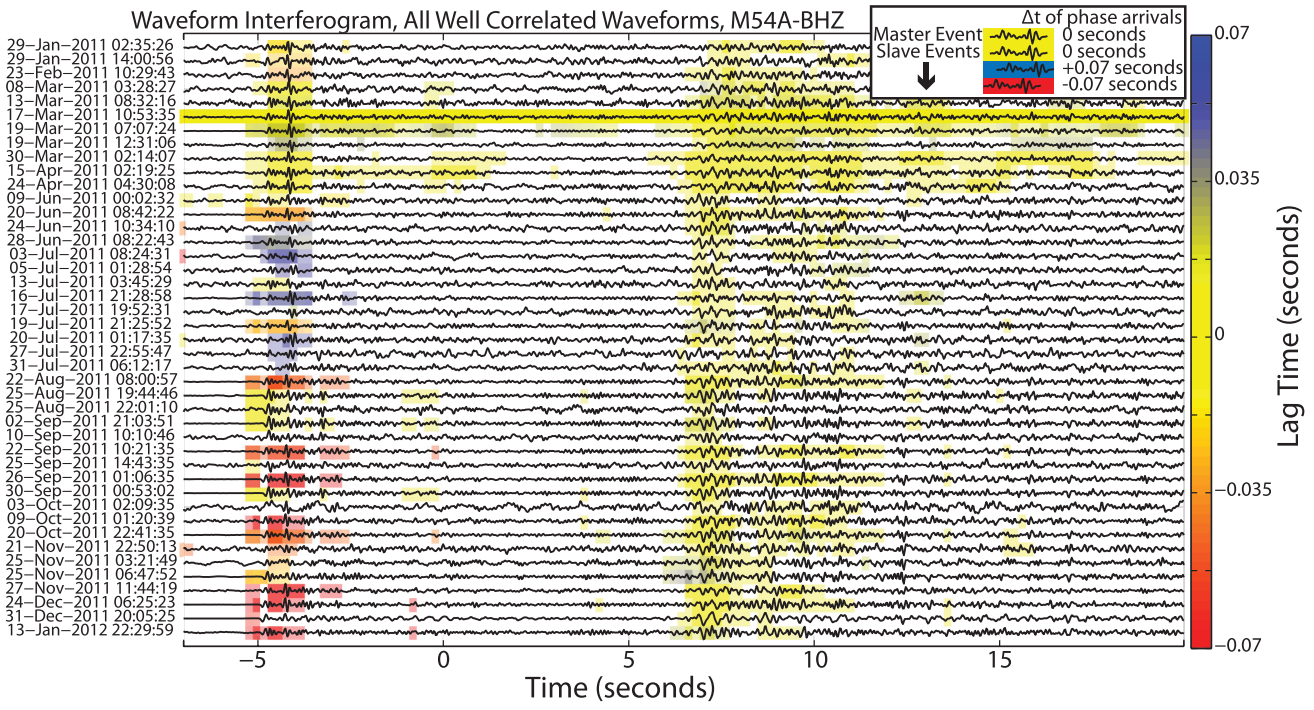

Figure 12. Example of a waveform interferogram for station-component M54A-BHZ calculated by GISMO between template 1 and the most correlated waveforms at this station. These waveforms are aligned based on crosscorrelation of the S-wave train between 6 and 15 s relative time. Any variations in the location will show up as an offset in the P-wave arrival near −4 s relative time, with negative lag (red) indicating larger S-P time presumably because of the event being farther from the station. Colors are only shown when correlation is above a threshold, such that only the template waveform is entirely yellow.

each other trace (Figure 12). This lag time corresponds to a ΔP and ΔS, which we use to calculate differential locations using the double-difference relocation algorithm HypoDD (Waldhauser and Ellsworth, 2000). To aid in placing these events in an absolute context, we use the absolute times of P and S arrivals at the four stations in the detector along with arrivals picked at an additional six seismic stations which clearly record each of the template earthquakes (Figure 13). We include the local short period seismic station YSUO, but the absolute location does not change considerably without it. The absolute locations of template earthquakes are calculated using elocate (Herrmann and Ammon, 2002), with a one-dimensional velocity model that is a hybrid of the locally determined shallow velocity model (Kim, 2013) and regionally determined deeper velocity model (Herrmann and Ammon, 2002), found through forward modeling to minimize location errors. The absolute locations are within 0.5 km (0.3 mi) of the well (stars, Figure 14), and the location of the December 31, 2011 M4.0 location is approximately 0.25 km (0.15 mi) northeast of the location obtained with a dense local network (Kim, 2013). Relative locations are adjusted according to these absolute locations, with Figure 14 showing the locations of 107 events with uncertainties less than 15 m (49 ft) in each direction. With our absolute locations, seismicity began near the injection well, but the initiation point would be almost directly beneath the well if we use the locally determined location of the December 31, 2011 event obtained by Kim (2013). The relative locations propagated to the west-southwest at a rate of approximately 1 to 2 km (0.6 to 1 mi) per yr, which would correspond to a triggering front through material that initially had $D \approx 5 \times 10^{-3}$ m^2/s. The delineation of seismicity is consistent with the east–west-trending nodal plane of the December 31 M4.0 earthquake and also with strikes of faults or fractures observed in the basement core samples from the injection well (ODNR, 2012).

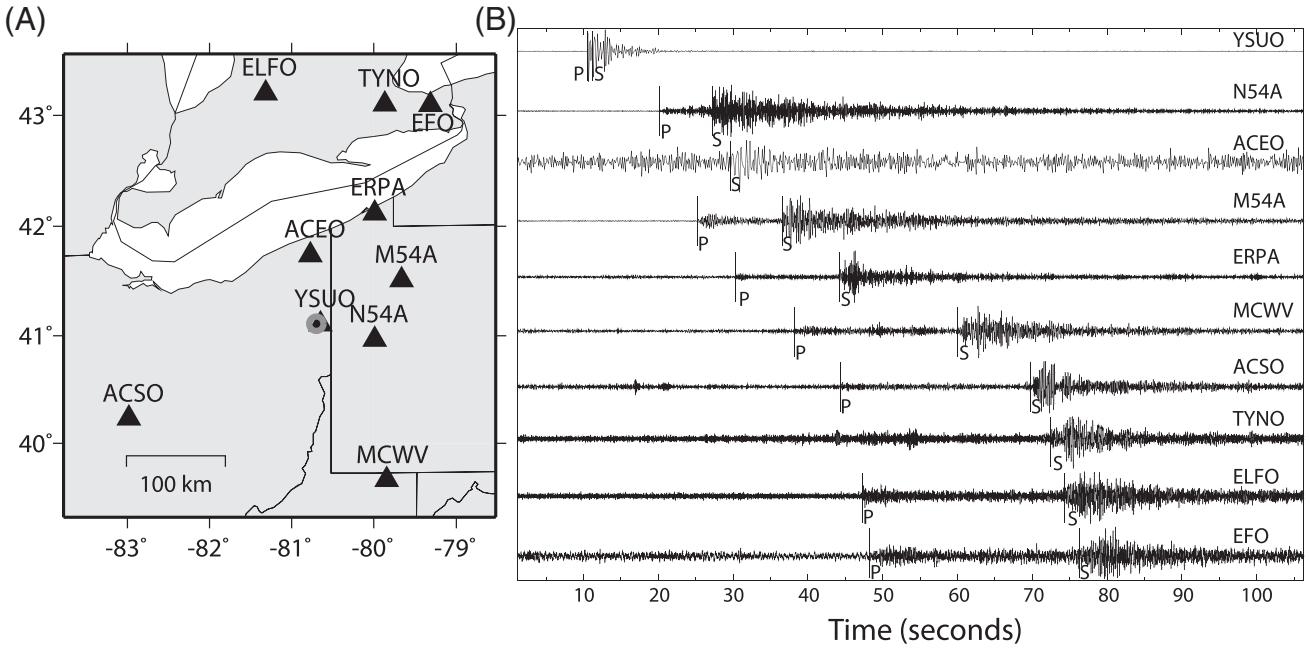

Figure 13. Station locations (left, black triangles) and P- and S-wave picks superimposed on the radiant wavefield (right), which were used to provide an absolute location (left, gray circle) of the December 31, 2011 M4.0 earthquake.

DISCUSSION

It is worth noting that, with the template matching technique described in the previous text, we would have been able to conclusively link this injection well with over 30 triggered earthquakes as early as the first earthquake large enough to make a template (March 17, 2011). We envision that, given a stable backbone monitoring network throughout the United States that is more dense than the current Advanced National Seismic System network but not necessarily as dense as the Earthscope Transportable Array, implementation of this technique could be essential in quickly and inexpensively diagnosing cases of induced seismicity and identifying responsible well sites and operational parameters before induced events reach potentially destructive magnitudes. In fact, a proposed 1-in-4 permanent retention of transportable array stations in the eastern and central United States (B. Woodward, 2013, personal communication) would provide a station spacing very similar to what we use in this study; therefore, we wholeheartedly support this proposed type of permanent monitoring network. With each additional "confirmed" case of induced seismicity, we get closer to understanding which conditions are necessary to induce larger seismic events. With this in mind, we investigated which conditions, if any, set this well apart from aseismic injection wells.

Results from analysis data from our relocations (as well as the ODNR and Lamont-Doherty local seismic array) indicate that the earthquakes originated from faults within Proterozoic igneous or metamorphic rocks beneath the injection interval (Kim, 2013). It is likely that fluids entered the fault from the zones of high porosity and permeability in the basement rocks identified in the deepest borehole geophysical logs, perhaps directly if the logged faults or fractures in fact represent the responsible fault. Pore fluid pressure then increased in discontinuous permeable zones of the fault system, reduced effective normal stress on these optimally oriented and critically stressed faults, and permitted fault slip to occur (Zoback and Harjes, 1997). The change in apparent diffusivity after arrival of the triggering front suggests development of more fully integrated fault zone permeability though time, increasing the area of potential fault failure and leading to the observed increase in magnitude with time. Drilling into the basement rocks and/or leaving that part of the well uncased during injection, thus giving fluids direct access to the fault zone, is what appears to set

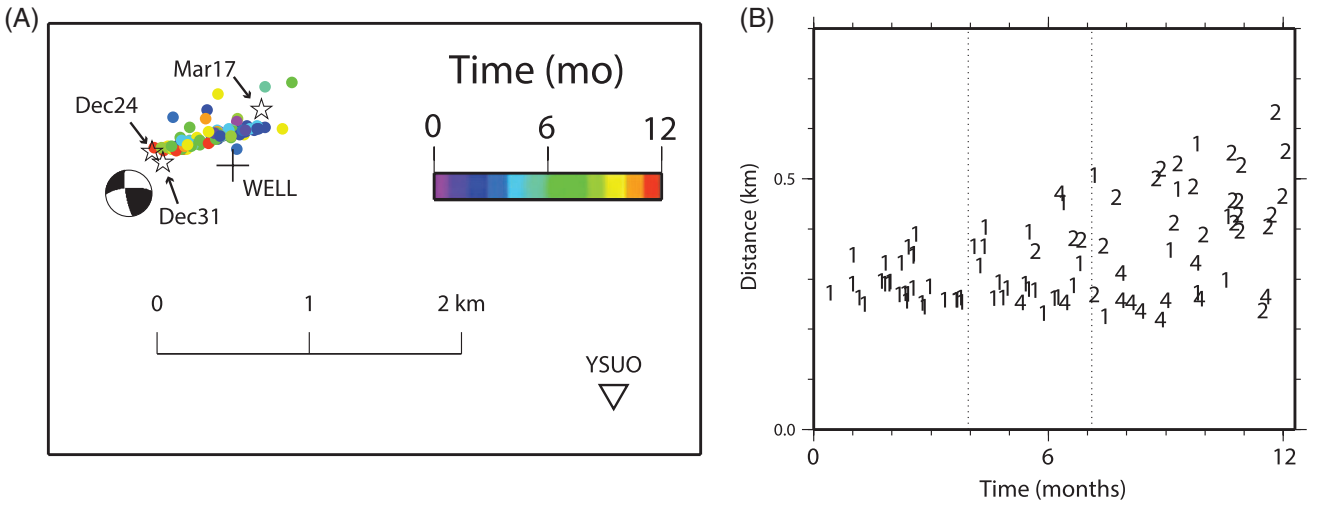

Figure 14. (A) Results of the joint absolute and relative relocation process, colored by time since January 1, 2011. Cross symbolizes the injection well, and the stars indicate the March 17, 2011, December 24, 2011, and December 31, 2011 earthquakes. There is likely a small amount of absolute location error, as Kim (2013) located the December 31 earthquake (focal mechanism shown as a beachball) several hundred meters to the southwest of our location (labeled star). Shifting our locations in this direction also brings the earliest earthquakes (cool colors) directly below the injection well. (B) Distance of the relocated events to the well, with the symbols (1, 2, or 4) representing the template that the relocated earthquake most closely matches. Here, we can see the expansion of hypocenters throughout the course of the sequence. Note, however, that a shift in the absolute locations will affect this graph.

this case apart from the many other wastewater injection wells in Ohio that have not induced such a sequence of earthquakes.

A time lag is expected from pore fluid pressure diffusion, which takes time to propagate into the surrounding rock volume (Shapiro et al., 2002). Initially, we envision that injection-related pore fluid pressure increased in discontinuous permeable zones of the fault system, reduced effective normal stress on these optimally oriented and critically stressed faults, and permitted fault slip to occur (Zoback and Harjes, 1997). Early displacement likely promoted fluid infiltration into adjacent, initially inaccessible regions of the fault, iteratively increasing the area of potential failure and allowing the source region for templates 2–4 earthquakes to fail. Following the initial stage, there is a direct relationship between the cumulative volume of injected wastewater and the cumulative number of earthquakes in the seismic sequence, suggesting development of more fully integrated fault zone permeability though time. Our hypothesis is reinforced by two observations: (1) The largest magnitude events ($M > 2$) were uncommon until after the midpoint of the sequence. We interpret this temporal relationship as indicating the point at which fault zone permeability achieved sufficient connectivity to induce rupture along greater (and adjacent) areas of the fault surface. (2) The triggered seismicity shows a clear time lag between injection and fault slip of 1–6 days (Figure 7), which we interpret to be a result of the pore pressure diffusion time.

Considering the evidence in favor of the source locations moving slightly over time, it suggests that new areas of the fault were becoming activated as additional fluid was pumped into the system. From this, it is not unreasonable to expect earthquakes to have occurred indefinitely, with the potential for opening up new areas of the fault to rupture. As more fault area becomes available, the maximum potential size of an earthquake increases, here supported by the observation that more than 99% of the moment release occurred in the final third of the sequence. Therefore, the increased injection volumes during this period likely increased the potential for a large seismic event.

CONCLUSIONS

We find that our template-matching approach is instrumental in building a catalog of events necessary

to studying the evolution of seismicity in the Youngstown region. We find very clear evidence that the earthquakes are directly caused by injection at the D&L Energy 1 Northstar well. Through our analysis, we also find evidence that source locations moved slightly, indicating that new areas of the fault were becoming activated as additional fluid was injected into the system. We attribute this to a positive feedback between pore fluid pressure allowing slip to occur, and slip allowing pore fluid pressure to infiltrate new areas of the fault. From this, it is not unreasonable to expect earthquakes to have occurred indefinitely, with the potential for opening up new areas of the fault to rupture. As more fault area becomes available, the maximum potential size of an earthquake increases, here supported by the observation that more than 99% of the moment release occurred in the second half of the sequence. Therefore, the increased injection volumes during this period likely increased the potential for a large seismic event. Although our technique can produce excellent results with the permanent seismic stations located in the United States, the operation of the Earthscope Transportable Array (of which M54A and N54A in Pennsylvania are a part) should greatly increase the return our technique delivers and has the potential to be an integral part of any investigation of triggered seismicity in the United States.

REFERENCES CITED

Ake, J., K. Mahrer, D. O'Connell, and L. Block, 2005, Deep-injection and closely monitored induced seismicity at Paradox Valley, Colorado: Bulletin of the Seismological Society of America, v. 95, no. 2, p. 664–683, doi:10.1785/0120040072.

Baranoski, M. T., 2007, Thickness and extent of saline Cambrian reservoirs in the Ohio region is controlled, in part, by the underpinning Precambrian complex and paleotopography: AAPG Eastern Section Annual Meeting Abstracts, Lexington, Kentucky, September 16–18, 2007, 27 p.

Baranoski, M. T., 2013, Structure contour map on the Precambrian unconformity surface in Ohio and related basement features (ver. 2.0): Columbus, Ohio, Ohio Department of Natural Resources, Division of Geological Survey Map PG-23, scale 1:500,000, 1 sheet, 17 p.

Buurman, H., and M. E. West, 2010, Seismic precursors to volcanic explosions during the 2006 eruption of Augustine Volcano, *in* J. A. Power, M. L. Coombs, and J. T. Freymueller, eds., The 2006 eruption of Augustine Volcano, Alaska: U.S. Geological Survey Professional Paper 1769, p. 41–57.

Calvert, W. L., 1974, Sub-Trenton structure of Ohio, with views on isopach maps and stratigraphic sections as basis for structural myths in Ohio, Illinois, New York, Pennsylvania, West Virginia, and Michigan: AAPG Bulletin, v. 58, no. 6, p. 957–972.

Deichmann, N., and D. Giardini, 2009, Earthquakes induced by the stimulation of an enhanced geothermal system below Basel (Switzerland): Seismological Research Letters, v. 80, no. 5, p. 784–798, doi:10.1785/gssrl.80.5.784.

Dorbath, L., N. Cuenot, A. Genter, and M. Frogneux, 2009, Seismic response of the fractured and faulted granite of Soultz-sous-Forêts (France) to 5 km deep massive water injections: Geophysical Journal International, v. 177, no. 2, p. 653–675, doi:10.1111/j.1365-246X.2009.04030.x.

El Hariri, M., R. E. Abercrombie, C. A. Rowe, and A. F. do Nascimento, 2010, The role of fluids in triggering earthquakes: Observations from reservoir induced seismicity in Brazil: Geophysical Journal International, v. 181, no. 3, p. 1566–1574, doi:10.1111/j.1365-246X.2010.04554.x.

Ellsworth, W. L., 2013, Injection-induced earthquakes: Science, v. 341, no. 6142, 7 p., doi:10.1126/science.1225942.

Frohlich, C., 2012, Two-year survey comparing earthquake activity and injection-well locations in the Barnett Shale, Texas: Proceedings of the National Academy of Sciences of the United States of America, v. 109, no. 35, p. 13,934–13,938, doi:10.1073/pnas.1207728109.

Gibbons, S. J., and F. Ringdal, 2006, The detection of low magnitude seismic events using array-based waveform correlation: Geophysical Journal International, v. 165, no. 1, p. 149–166, doi:10.1111/j.1365-246X.2006.02865.x.

Hansen, M. C., and L. J. Ruff, 2003, The Ohio seismic network: Seismological Research Letters, v. 74, no. 5, p. 561–564, doi:10.1785/gssrl.74.5.561.

Herrmann, R., and C. J. Ammon, 2002, Computer programs in seismology version 3.20: Surface waves, receiver functions, and crustal structure: St. Louis, Missouri, St. Louis University, 110 p.

Hitzman, M., D. Clarke, E. Detournay, J. Dietrich, D. Dillon, S. Green, and C. Gibbs, 2012, Induced seismicity potential in energy technologies: Washington, DC, National Academies Press, 239 p.

Horton, S., 2012, Disposal of hydrofracking waste fluid by injection into subsurface aquifers triggers earthquake swarm in central Arkansas with potential for damaging earthquake: Seismological Research Letters, v. 83, no. 2, p. 250–260, doi:10.1785/gssrl.83.2.250.

Keranen, K. M., H. M. Savage, G. A. Abers, and E. S. Cochran, 2013, Potentially induced earthquakes in Oklahoma, USA: Links between wastewater injection and the 2011 Mw 5.7 earthquake sequence: Geology, v. 41, no. 6, p. 699–702, doi:10.1130/G34045.1.

Kim, W.-Y., 2013, Induced seismicity associated with fluid injection into a deep well in Youngstown, Ohio: Journal of Geophysical Research: Solid Earth, v. 118, no. 7, p. 3506–3518, doi:10.1002/jgrb.50247.

Mazzotti, S., and J. Townend, 2010, State of stress in central and eastern North American seismic zones: Lithosphere, v. 2, no. 2, p. 76–83, doi:10.1130/L65.1.

McGarr, A., D. Simpson, and L. Seeber, 2002, Case histories of induced and triggered seismicity, *in* W. H. K. Lee, H. Kanamori, P. C. Jennings, and C. Kisslinger, eds., International handbook of earthquake and engineering seismology: New York, Academic Press, v. 81A, p. 647–661.

Nicholson, C., and R. L. Wesson, 1990, Earthquake hazard associated with deep well injection: A report to the U.S. Environmental Protection Agency: U.S. Geological Survey Bulletin 1951, accessed May 19, 2015, http://pubs.usgs.gov/bul/1951/report.pdf.

Nicholson, C., and R. L. Wesson, 1992, Triggered earthquakes and deep well activities: Pure and Applied Geophysics, v. 139, no. 3–4, p. 561–578, doi:10.1007/BF00879951.

ODNR, 2012, Preliminary report on the Northstar 1 Class II injection well and the seismic events in the Youngstown, Ohio, area: Columbus, Ohio, Ohio Department of Natural Resources, 24 p.

Parotidis, M., 2004, Back front of seismicity induced after termination of borehole fluid injection: Geophysical Research Letters, v. 31, no. 2, L02612, 5 p., doi:10.1029/2003GL018987.

Parotidis, M., 2005, Evidence for triggering of the Vogtland swarms 2000 by pore pressure diffusion: Journal of Geophysical Research, v. 110, no. B5, B05S10, 12 p., doi:10.1029/2004JB003267.

Peng, Z., and P. Zhao, 2009, Migration of early aftershocks following the 2004 Parkfield earthquake: Nature Geoscience, v. 2, no. 12, p. 877–881, doi:10.1038/ngeo697.

Raleigh, C. B., J. H. Healy, and J. D. Bredehoeft, 1976, An experiment in earthquake control at Rangely, Colorado: Science, v. 191, no. 4233, p. 1230–1237, doi:10.1126/science.191.4233.1230.

Reyes, C. G., and M. E. West, 2011, The waveform suite: A robust platform for manipulating waveforms in MATLAB: Seismological Research Letters, v. 82, no. 1, p. 104–110, doi:10.1785/gssrl.82.1.104.

Ryder, R. T., M. H. Trippi, C. S. Swezey, R. D. Crangle, Jr., R. S. Hope, E. L. Rowan, and E. E. Lentz, 2012, Geologic cross section C–C' through the Appalachian basin from Erie County, north-central Ohio, to the Valley and Ridge province, Bedford County, south-central Pennsylvania: U.S. Geological Survey Scientific Investigations Map 3172, 2 sheets, 70 p.

Seeber, L., J. G. Armbruster, and W.-Y. Kim, 2004, A fluid-injection-triggered earthquake sequence in Ashtabula, Ohio: Implications for seismogenesis in stable continental regions: Bulletin of the Seismological Society of America, v. 94, no. 1, p. 76–87, doi:10.1785/0120020091.

Shapiro, S. A., and C. Dinske, 2009, Fluid-induced seismicity: Pressure diffusion and hydraulic fracturing: Geophysical Prospecting, v. 57, no. 2, p. 301–310, doi:10.1111/j.1365-2478.2008.00770.x.

Shapiro, S. A., O. S. Kruger, C. Dinske, and C. Langenbruch, 2011, Magnitudes of induced earthquakes and geometric scales of fluid-stimulated rock volumes: Geophysics, v. 76, no. 6, p. WC55–WC63, doi:10.1190/geo2010-0349.1.

Shapiro, S. A., R. Patzig, E. Rothert, and J. Rindshwentner, 2003, Triggering of seismicity by pore-pressure perturbations: Permeability-related signatures of the phenomenon: Pure and Applied Geophysics, v. 160, no. 5, p. 1051–1066, doi:10.1007/PL00012560.

Shapiro, S. A., E. Rothert, V. Rath, and J. Rindschwentner, 2002, Characterization of fluid transport properties of reservoirs using induced microseismicity: Geophysics, v. 67, no. 1, p. 212–220, doi:10.1190/1.1451597.

Shelly, D. R., G. C. Beroza, and S. Ide, 2007, Non-volcanic tremor and low-frequency earthquake swarms: Nature, v. 446, no. 7133, p. 305–307, doi:10.1038/nature05666.

Shelly, D. R., and J. L. Hardebeck, 2010, Precise tremor source locations and amplitude variations along the lower-crustal central San Andreas Fault: Geophysical Research Letters, v. 37, no. 14, L14301, 5 p., doi:10.1029/2010GL043672.

Simpson, D., 1986, Triggered earthquakes: Annual Review of Earth and Planetary Sciences, v. 14, no. 1, p. 21–42, doi:10.1146/annurev.ea.14.050186.000321.

Skoumal, R. J., M. R. Brudzinski, B. S. Currie, and J. Levy, 2014, Optimizing multi-station earthquake template matching through re-examination of the Youngstown, Ohio, sequence: Earth and Planetary Science Letters, v. 405, p. 274–280, doi:10.1016/j.epsl.2014.08.033.

Townend, J., and M. D. Zoback, 2000, How faulting keeps the crust strong: Geology, v. 28, no. 5, p. 399–402, doi:10.1130/0091-7613(2000)28<399:HFKTCS>2.0.CO;2.

Van der Elst, N. J., H. M. Savage, K. M. Keranen, and G. A. Abers, 2013, Enhanced remote earthquake triggering at fluid-injection sites in the Midwestern United States: Science, v. 341, no. 6142, p. 164–167, doi:10.1126/science.1238948.

Waldhauser, F., and W. L. Ellsworth, 2000, A double-difference earthquake location algorithm: Method and application to the Northern Hayward Fault, California: Bulletin of the Seismological Society of America, v. 90, no. 6, p. 1353–1368, doi:10.1785/0120000006.

Wickstrom, L. H., E. R. Venteris, J. A. Harper, J. McDonald, E. R. Slucher, K. M. Carter, S. F. Greb, et al., 2005, Characterization of geologic sequestration opportunities in the MRCSP region—Phase I task report: Ohio Department of Natural Resources, Division of Geological Survey, Open File Report 2005-1, 152 p., accessed May 2015, http://geosurvey.ohiodnr.gov/portals/geosurvey/PDFs/OpenFileReports/OFR_2005-1.pdf.

Zoback, M. D., and H.-P. Harjes, 1997, Injection-induced earthquakes and crustal stress at 9 km depth at the KTB deep drilling site, Germany: Journal of Geophysical Research, v. 102, no. B8, p. 18,477–18,491, doi:10.1029/96JB02814.

Zoback, M. L., 1992, Stress field constraints on intraplate seismicity in eastern North America: Journal of Geophysical Research: Solid Earth, v. 97, no. B8, p. 11,761–11,782, doi:10.1029/92JB00221.